DESCRIPTIVE NOTES - HYPERSPECTRAL

INTRODUCTION

For geological mapping applications, hyperspectral remote sensing instruments (or imaging spectrometers) can provide significant advantages over traditional optical imaging systems such as Landsat, or radar imaging systems such as RADARSAT-1. The higher spectral resolution in hyperspectral data sets allows for the identification of specific minerals or rocks groups in some cases as opposed to general discrimination between some rock units that other sensors are able to provide. Reflectance properties of minerals have been well studied (e.g. Hunt and Salisbury 1970, 1971; Hunt 1977; Goetz et al., 1982; Clarke et al., 1990) although fewer studies have been conducted on the reflectance spectra of rocks (e.g. Hunt et al., 1973a, 1973b, 1974). Significant research in hot desert areas of the world have shown that a wide range of minerals, particularly clays, hydroxyl group minerals and carbonates can be uniquely identified and mapped through spectral analysis (*see* van der Meer and de Jong 2002 and references therein). Much less research has been conducted in cold-desert environments typical of Canada's North (e.g. Cloutis 1992). Recent work using airborne hyperspectral (Probe-1) data in the Canadian Arctic, however, indicates that dolostones can be uniquely separated from limestones (Budkewitsch et al., 2000) and that metasedimentary, metatonalitic and metagabbroic rocks can be discriminated (Harris et al., 2001; Harris et al., 2005). A study by Bowers and Rowen (1996) using hyperspectral data acquired by the Jet Propulsion Laboratory's AVIRIS sensor over the Ice River alkaline complex of British Columbia indicated that several lithologies could be discriminated and identified.

Arctic environments offer great promise for the application of hyperspectral remote sensing for geologic mapping due to the lack of ubiquitous vegetation cover. However even under these favourable conditions, remote sensing (including hyperspectral) applications face numerous challenges. These include, (1) the presence of lichens, (2) weathering (both mechanical and chemical), (3) the mechanical break down of lithologies into boulder fields which may not provide a homogeneous target for remote sensing, and (4) lithologies that are characterized by a range of minerals. Other challenges include low sun illumination angles, shadows and cloud cover. The main focus of hyperspectral research for geological applications has been the identification of specific minerals or rock types, pure expressions of which in hyperspectral data sets are sometimes referred to as spectral end-members. An initial small pilot study was conducted by Harris et al., (2005) in the south-eastern region of Baffin Island to test the applicability of hyperspectral data for geologic mapping. Results were encouraging enough to warrant a larger survey over a larger section of Baffin Island.

This Open File provides some overall results on a hyperspectral survey that acquired approximately 9,000 km² of airborne data during the summer of 2004 over southern Baffin Island to further evaluate its value for supporting regional mapping efforts. The maps (White Bear Bay, Robert Point, Canon Inlet, Livingstone River, and Soper Lake) illustrate one possible result for providing hyperspectral map units derived from specialized processing of the data by A.U.G. Signals Ltd. in conjunction with Natural Resources Canada.

The maps produced in these Open Files (5051, 5052, 5053, 5054 and 5055) represent a new method for creating predictive maps of lithological units from remotely sensed data. The colours seen on each map represent spectral classes that exhibit characteristics similar to training sites selected from 12 representative lithological units mapped by the Geological Survey of Canada shown on maps 1979A–1985A (St-Onge et al., 2001). These representative areas were selected by consulting the GSC 1:100,000 scale geology maps, Landsat imagery and available mineral assessment reports. Spectra were generated for each training site and used as input to A.U.G. Signals' HE/LP (Hyperspectral Exploration/Lithological Processing) algorithm, which produced abundance values for each lithological class. The resulting colours on the map represent areas with a high confidence in the match with the training spectra. Many areas appear unmapped for two reasons, (1) only areas of exposed rock where analysed, thus areas of snow, ice, water, vegetation and thick till were excluded and, (2) only areas above a high threshold match to the training areas were included in the resulting map.

DATA ACQUISITION

Survey Location

The Meta Incognita Peninsula of southern Baffin Island was selected by the GSC as the location to conduct a regional airborne hyperspectral survey (Fig.1) in order to generate a first-order predictive geological map.

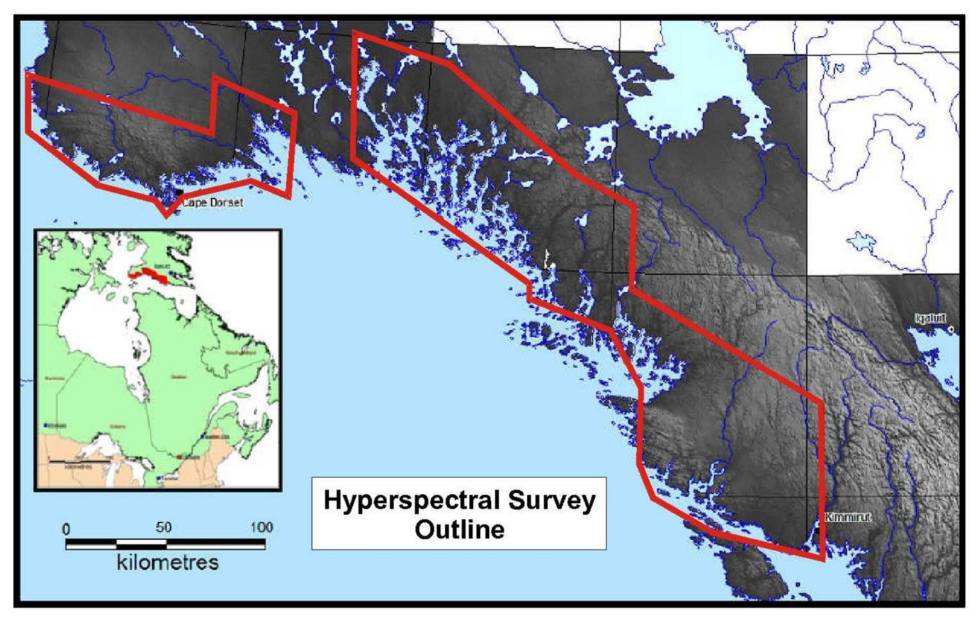

Figure 1. Outline of PROBE Hyperspectral Survey (planned).

Probe-1 Hyperspectral Sensor

The Probe-1 Imaging Spectrometer (Fig. 2) was built by Integrated Spectronics Ltd. The Probe-1 is a whiskbroom style instrument that collects data in a cross-track direction by mechanical scanning and in an along-track direction by movement of the airborne platform. The sensor is operated in an un-pressurized twin-engine aircraft, fitted with standard aerial photography camera mounts and survey ports. Daily data acquisition for this survey ranged from about 1,500–3,000 km² per day, depending on distance from the base of operations, weather conditions and sun angle limitations.

The instrument records 512 cross-track pixels, each sampling 128 wavelength bands of reflected electromagnetic radiation in the visible to short-wave infrared range (400 to 2,450 nanometres). Band positioning and band widths range between 15–20 nanometres. In the visible-near infrared (VNIR) and short-wave infrared (SWIR), the at-sensor radiance is dispersed by four spectrometers onto four detector arrays.

To avoid geometric distortions in the recorded imagery, the Probe-1 spectrometer was mounted on a three axis, gyro-stabilized mount. The gyro-stabilized platform provides dynamic compensation to the sensor system to correct for angular aircraft movements (roll, pitch, and yaw). The platform maintains the image plane of the sensor to near-horizontal and dampens aircraft vibration for the sensor system. The stabilized platform significantly improves the quality of the data acquired.

Geolocation of image pixels is accomplished using the GPS data as well as a C-MIGITS inertial measurement unit (IMU) that provides data on aircraft attitude. The C-MIGITS IMU unit is located upon the body of the sensor casing. The IMU records the residual aircraft/sensor movement after compensation by the stabilized platform. The C-MIGITS IMU outputs information to a separate log file that includes the GPS and IMU data required for geocorrection of the image data.

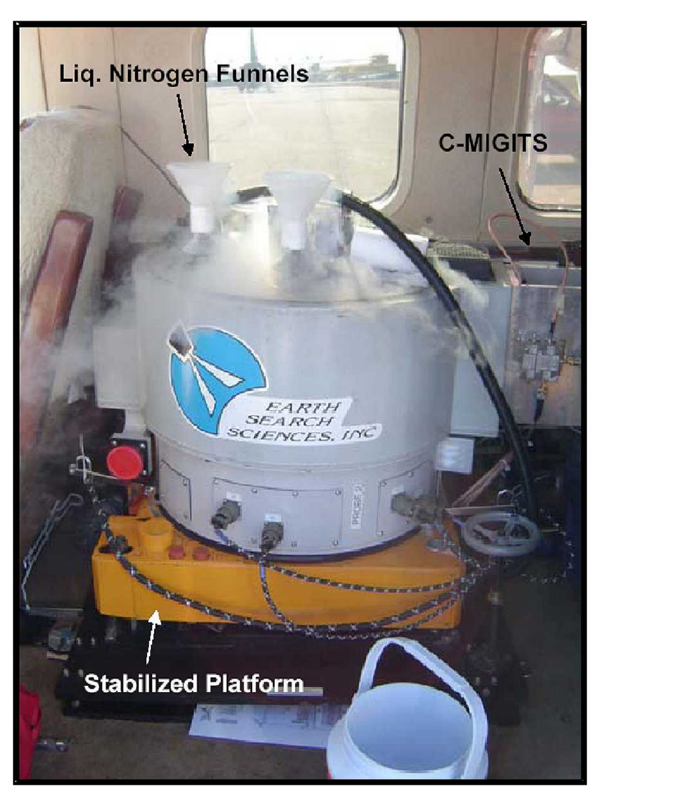

Figure 2. PROBE Hyperspectral Sensor.

Illumination Conditions (Sun Angles)

Solar noon for Iqaluit (63.750° N, 68.517° W) for the month of August 2004 was at approximately 12:40 local time. The survey plan was to have the aircraft at altitude and on-site between to collect data for approximately four-hour periods at ±2 hours of solar noon. Daily maximum sun elevations ranged from 45 degrees for the week of July 26 to 37.5 degrees on August 22.

Flying Specifications

The flight lines range in length from 20–70 km and are spaced about 3.8 km apart. A 30% overlap requirement was specified to mitigate against data gaps between adjacent flight lines. The flight-line layout was designed to meet the following four key criteria:

1. To provide approximately 10 m ground instantaneous field of view (GIFOV), an aircraft altitude of 15,200 feet and flight line spacing of 3.8 km was used.
2. To minimize bi-directional reflectance, flight lines were orientated in approximately north-south directions.
3. No greater than a 10% cloud cover per flight line was deemed to be acceptable for inclusion in the final map.
4. Data were collected with a minimum solar elevation angle of 35 degrees, thus most surveying was carried out within 2 hours of solar noon.

Mission

The survey crew was on-site in Iqaluit for a total of 25 days from July 30 to August 23. 46 survey lines were flown during that time, for a total coverage (net) of 9,697 km². The actual area of the proposed survey block is shown in Figure 3. Weather conditions were generally poor over this four-week period in 2004 where for the majority of the time, south Baffin Island was under overcast/broken cloud conditions. This worked against completing the target coverage of 30,000 km².

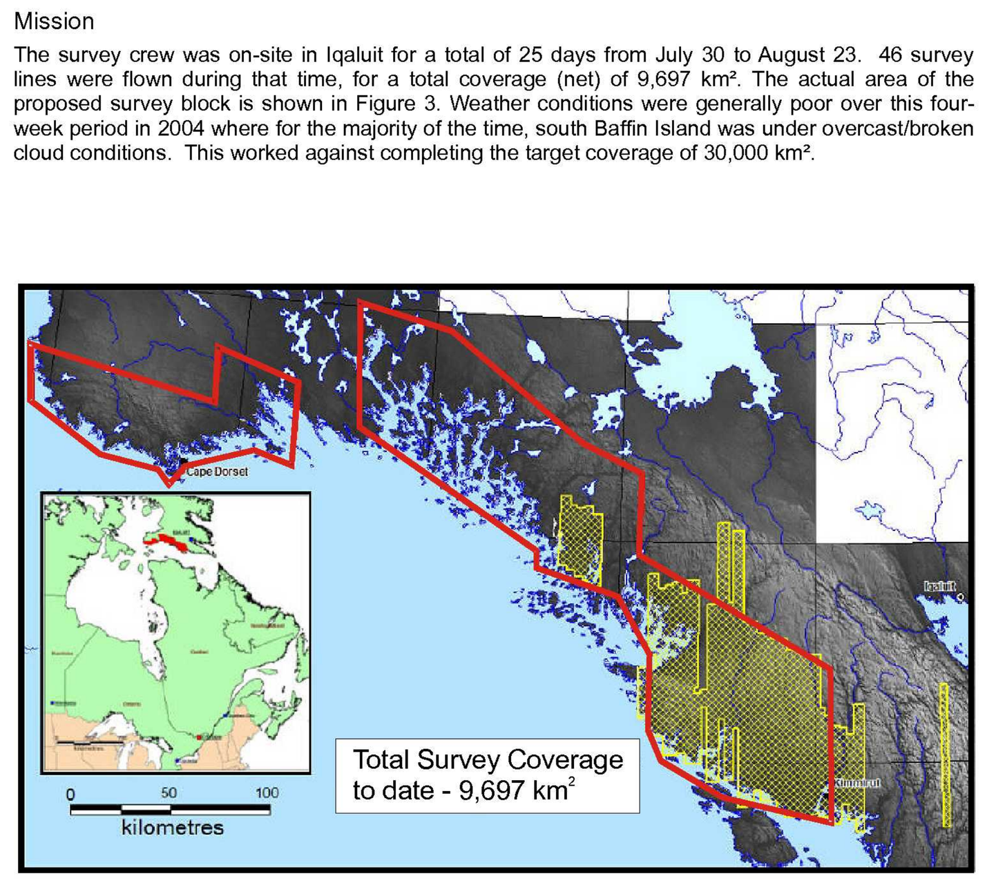

Figure 3. Outline of PROBE Hyperspectral Survey (actual area covered).

DATA PROCESSING

Image data obtained from the Probe-1 scanner is received as unprocessed, flat binary files stored in Band Interleaved by Line (BIL) format with an associated ENVI™ image analysis system compatible ASCII header file. Along with the raw hyperspectral data cube, five additional files are included: dark current and on-board lamp calibration data; ASCII log and sensor files (which log system performance during operation); and an ASCII GPS/IMU file listing the positioning information for each nadir pixel.

Data pre-processing encompasses three main processing steps: transformation of the raw data to radiance-at-sensor (radiometric correction); orthorectification (geometric correction); and transformation to surface reflectance (atmospheric correction) (Fig. 4).

A.U.G. Signals' HE/LP (Hyperspectral Exploration/Lithological Processing) algorithm was used for all mineral mapping, detection, and classification. This advanced data processing technique can automatically detect and classify minerals from hyperspectral data and provide reliable results by displaying confidence levels of the achieved detection results. The HE/LP algorithms include two processes:

- ***mineral detection*** - A fully adaptive orthogonal projection technique is optimized and used for specific mineral and lithological spectral detection
- ***mineral classification*** - An Evidential Reasoning approach (the Dempster- Shafer method) has been employed to estimate the confidence levels of detected end members

A.U.G. Signals' adaptive orthogonal projection technique does not require all mineral signatures or end members in the image scene in order to estimate the abundance images for the minerals of interest. The method has been improved from its original form (A.U.G. Signals 2003) by optimally fusing in the least square sense with other clutter suppression techniques including adaptive matched filtering, Kelly detector, and orthogonal subspace detector etc. (Duda et al. 2001; Kelly 1998; Harsanyi and Chang 1994). The HE/LP algorithm attempts to find the weighting coefficients for different spectral bands, and obtain an abundance image for any given target/mineral spectral signature. To achieve this objective, HE/LP suppresses the background (i.e. materials that are considered as interference). The projection coefficients will be different for each spectral signature and will result in an abundance image that uniquely characterizes the specific mineral of interest. The results have higher probabilities of detection, while keeping the probability of false alarm under a certain predefined value. This provides rapid means of detecting specific minerals from their spectral signatures, which may be obtained from spectral libraries or image-derived spectra.

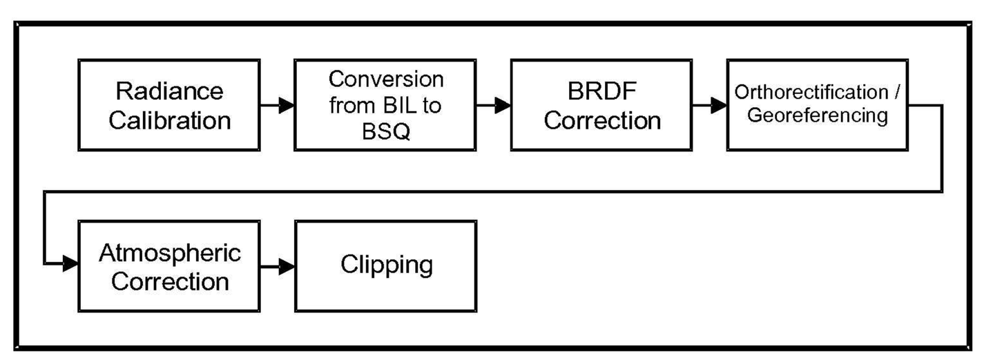

Figure 4. Hyperspectral data processing.

The general procedures of the adaptive orthogonal projection technique are described as follows:

1. Select background pixels from the image scene for a given target/mineral spectral signature;
2. Compute the projection coefficients for all spectral bands so that the abundance value for the given target spectral signature is very high while the abundance values for the background pixels are very low;
3. Remove the background pixels with relatively high abundance values from the training background set;
4. Repeat the steps 2 and 3 until probability of detection and the probability of false alarm satisfy a certain cut-off value;
5. Calculate the abundance values for all pixels in the image using the finally obtained projection coefficients;
6. Repeat steps 1 to 5 for each mineral spectral signature.

Background pixels are selected to estimate the presence of minerals and to suppress background clutter. More than a thousand background pixels are usually employed in the processing. HE/LP uses an iterative process to ensure the proper selection of the background pixels. The resulting abundance images are independent to each other and do not have any constraints. Furthermore, the summation of the abundance values of a pixel from all minerals is not equal to 1 as in the constrained linear spectral unmixing algorithm.

The HE/LP algorithm implements a unique approach to confidence level estimation of the detected minerals. The abundance values represent relative strengths of the material of interest that exists in the image scene. In order to obtain the final desired confidence levels, decisions (probabilities) from all detections (abundance images) have to be considered. The Dempster-Shafer (Evidential Reasoning) method (Shafer 1976) is employed to combine all probabilities from all decision sources and to obtain the final confidence levels. It is a method that generalizes the Bayesian inference (Dempster 1968; Lein 2003). By using the evidential reasoning approach for representing and combining data in the multiple decision application, each decision source (abundance image of different spectral signature) is allowed to contribute information at its own level of detail. The evidential reasoning structure is general enough to fully utilize each decision regardless of its form. It also handles the problem of incomplete or uncertain decisions. In the final confidence images, all pixel values are constrained. The value represents the confidence/probability of the detected mineral's presence in the given pixel.

The estimation of the confidence levels using the Dempster-Shafer (Evidential Reasoning) method is described as follows. Assume that we have a set of M minerals or materials of interest, such that a target pixel is type $s_1, s_2, \ldots, s_M$, or s_{M+1}, where s_{M+1} is a material that does not belong to $s_1, s_2, \ldots$, and s_M.

1. For each abundance image of a material of interest, the statistics of the image, such as the mean and covariance matrix, are estimated;
2. The probability masses of all pixels in an abundance image are estimated based on a multi-variant Gaussian distribution;
3. The probability masses from all different abundance images/decisions are combined using the Dempster's rules (Shafer, 1968);
4. The final M+1 confidence levels for all pixels are obtained.

A.U.G. Signals' HE/LP algorithms have been automated using a batch script to process large amounts of data without human interaction.

The automatic procedures for A.U.G. Signals' HE/LP are described as follows. The projection coefficients are obtained for each spectral signature from the data cube where the spectral signature is extracted. These projection coefficients and the spectral signatures are then used to process all data cubes to obtain the abundance images for the specific material. The process is repeated for all spectral signatures. The confidence images are then determined using the Dempster-Shafer evidence reasoning method by combining all abundance images of all spectral signatures.

The spectral signatures of materials of interest used in HE/LP were extracted form the reflectance data cube based on ground truth information. The selection of training areas, or regions of interest (ROIs), used to build the reference spectral library was guided by 1:100,000 scale GSC maps (Fig. 5) and information available within mineral assessment reports (Fig. 6). The reflectance spectra under each ROI were averaged to produce library spectra to be used in the mineral/lithological mapping process. The following criteria were used to select the location of the ROI's:

- guided by GSC and / or mineral assessment reports.
- areas of outcrop were used (visually interpreted using air photos and Landsat data); generally > 1000 pixels (> 100,000 m2) to create an average spectra - in some cases (e.g. gossans) only a few pixels (< 10) were sampled.
- where two spectra for the same material were collected, an average was used.
- areas of vegetation, water, snow, ice, cloud and till cover were avoided.

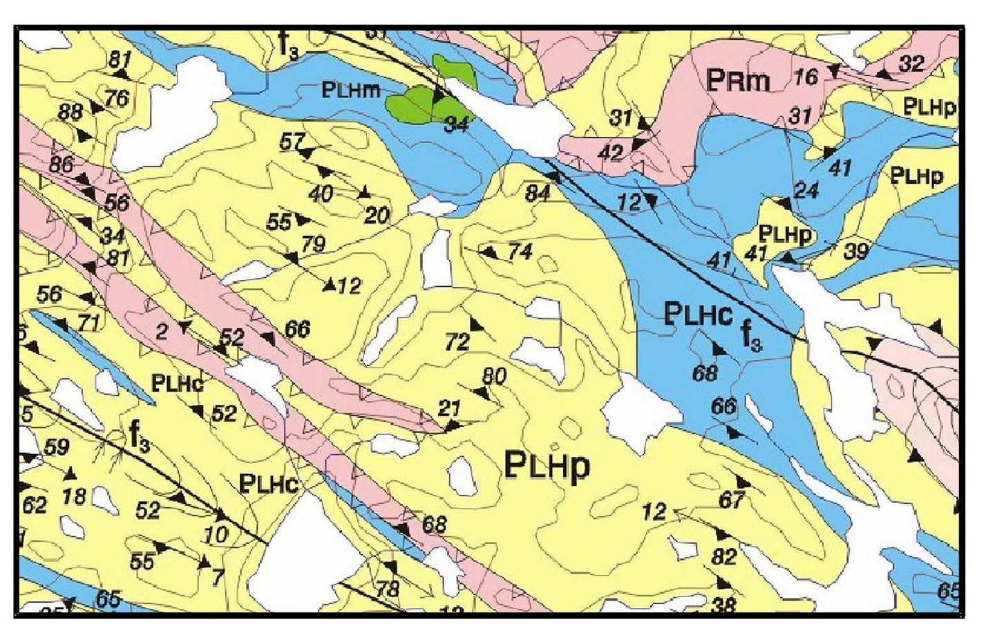

Figure 5. Example of 1:100 000 scale geological map used to define regions of interest (ROI) for the collection of spectral signatures for each rock type.

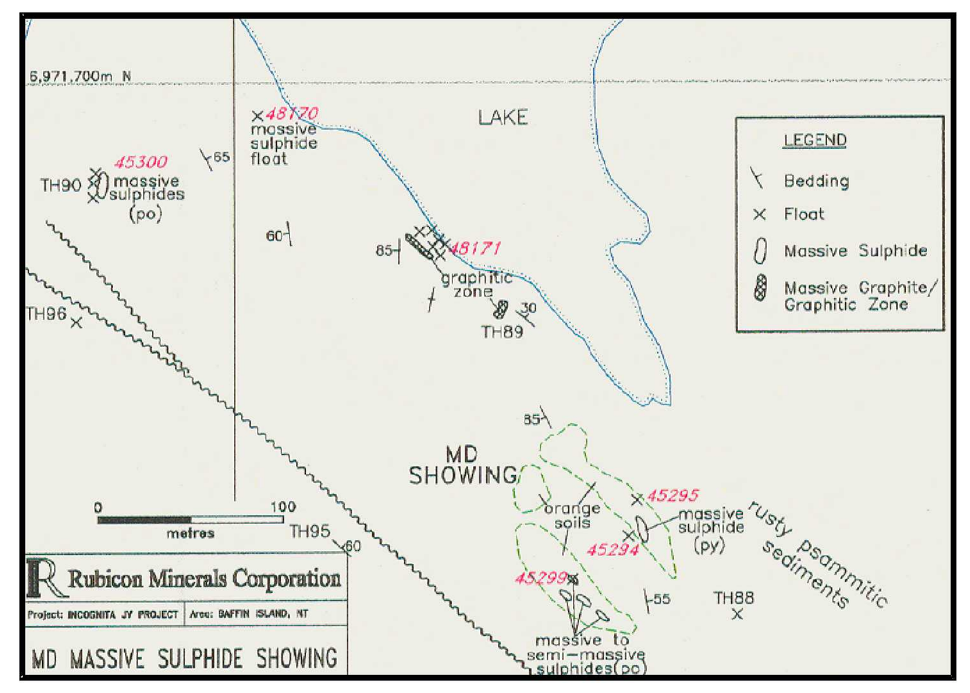

Figure 6. Example of Mineral Assessment Report used to define regions of interest (ROI) for the collection of spectral signatures for each rock type.

Twelve (12) key lithologies and two different gossans were selected to generate interpreted mineral and lithology maps for the survey coverage.

- Two different gossans discovered and reported by Rubicon Resources (Rubicon Resources, 1996).
- Eleven Proterozoic age lithological units of the Superior Province as mapped and reported by the GSC (St-Onge et al., 2001):

<u>Cumberland Batholith</u>

1. Pyroxene monzogranite to syenogranite (PCmo)

<u>Blandford Bay Assemblage</u>

2. Metaperidotite, metagabbro, metapyroxenite (PBBm)
3. Metaquartzite (PBBq)
4. Psammite and semipelite (PBBp)

<u>Lake Harbour Group</u>

5. White biotite-garnet monzogranite (PLHw)
6. Metaleucodiorite, metatonalite (PLHd)
7. Metagabbro, amphibolite (PLHm)
8. Marble, calc-silicate (PLHc)
9. Psammite and semipelite (PLHp)
10. Pyroxene-biotite monzogranite-tonalite orthogneiss and associated rocks (PRm)
11. Pyroxene-biotite monzogranite and associated rocks (PNm)

<u>Other</u>

12. Unknown sedimentary unit

Where possible, reference spectra for each lithology were collected unique to each day of the data acquisition. For example, reference library spectra for psammite/semipelite of the Lake Harbour Group (PLHp) were collected and averaged for each survey day individually. This resulted in three different PLHp spectra, one for each survey day (August 5, 10, and 12). This method helped reduce error in the mineral/ lithology mapping process attributed to variance in both geology and reflectance intensity across lines. Figure 7 shows an example of reference spectra for a number of lithologies on August 10, 2004. Spectra for ultramafic rocks such as metaperidotite, metapyroxenite and metadunite were not collected as it was difficult to locate nearby outcrops of these rocks due to their spatially restricted nature. To map these rocks, ground-truthing would be advantageous so that the exact pixels comprising these rocks can be located.

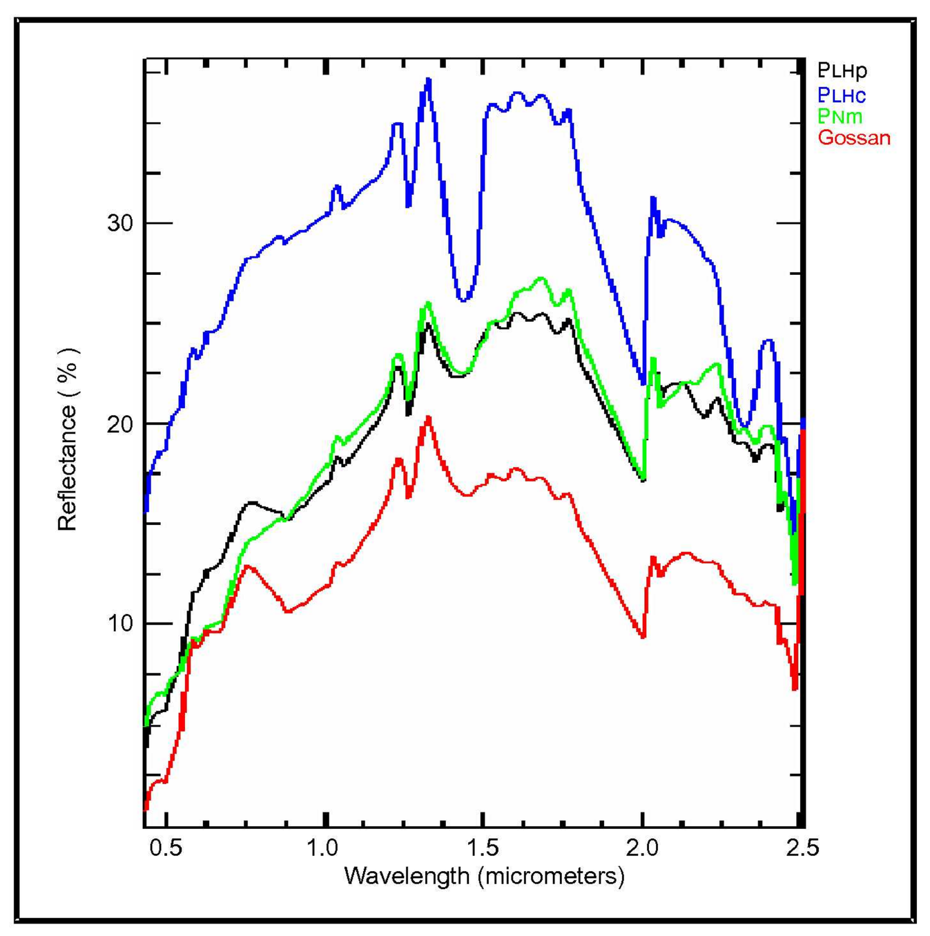

Figure 7. Reference spectra of major rock types used for classification.

Abundance and Confidence Analysis and Interpretation

The HE/LP algorithms produce an abundance image for each input library spectra. Depending on the material referenced, not all abundance images are included in the confidence calculation. For example, materials such as gossan are expected in only limited amounts relative to lithological units. Gossan, therefore, was not included in the confidence analysis. Gossan was mapped using the abundance images. The reference lithologies for the rule classification were reclassified into ten units (Fig. 8) without an age distinction to the following:

1. Areas of strong iron oxidization (formally gossan)
2. White granite (formerly PLHw)
3. Granitoid type 1 (formerly PNm)
4. Granitoid type 2 (formerly PCmo and/or PRm)
5. Carbonate rocks (PLHc)
6. Psammite, semipelite (formerly PLHp and/or the psammitic sub-unit of PBBp)
7. Other sedimentary rocks (unknown sedimentary rock)
8. Quartzite (formerly the silicic sub-unit of PBBp)
9. Leucodiorite, tonalite (formerly PLHd)
10. Mafic rocks (formerly PLHm)

The final mineral and interpreted lithological maps were mosaiced and output to GeoTIFF format. The GeoTIFF format allows the data to be easily incorporated into the GIS system for cartographic output (i.e. printed map products). The GeoTIFF format was also used as an input into the Geoscience Data Repository (GDR). In summary, Figure 9 provides an overview of the process going from reflectance data to a classified GeoTIFF image file. These data are displayed on the companion Open File maps.

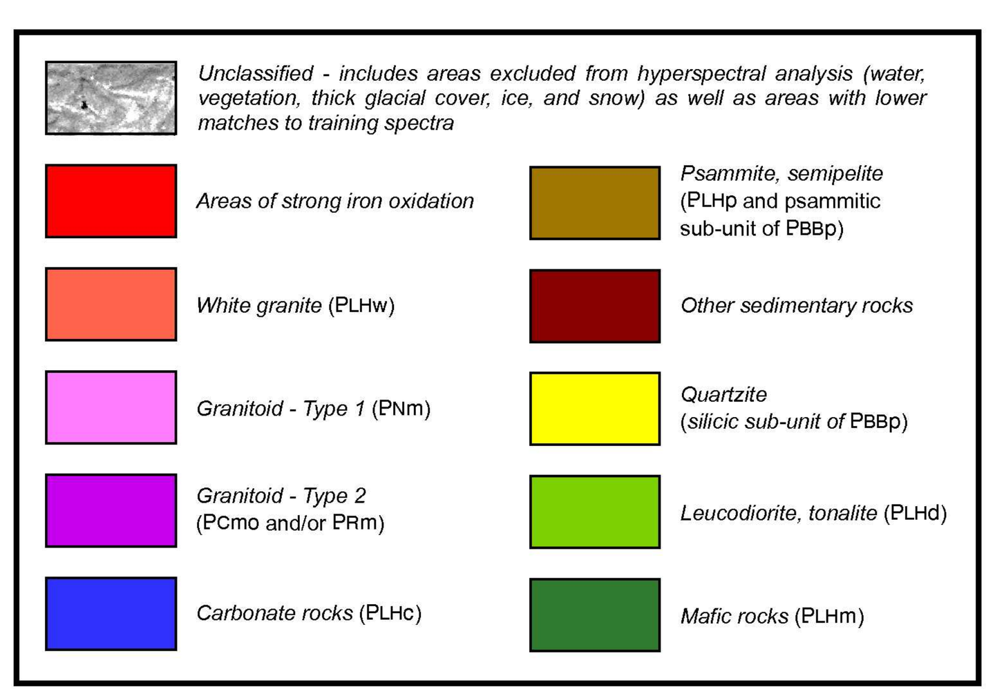

Figure 8. Legend for Hyperspectral maps.

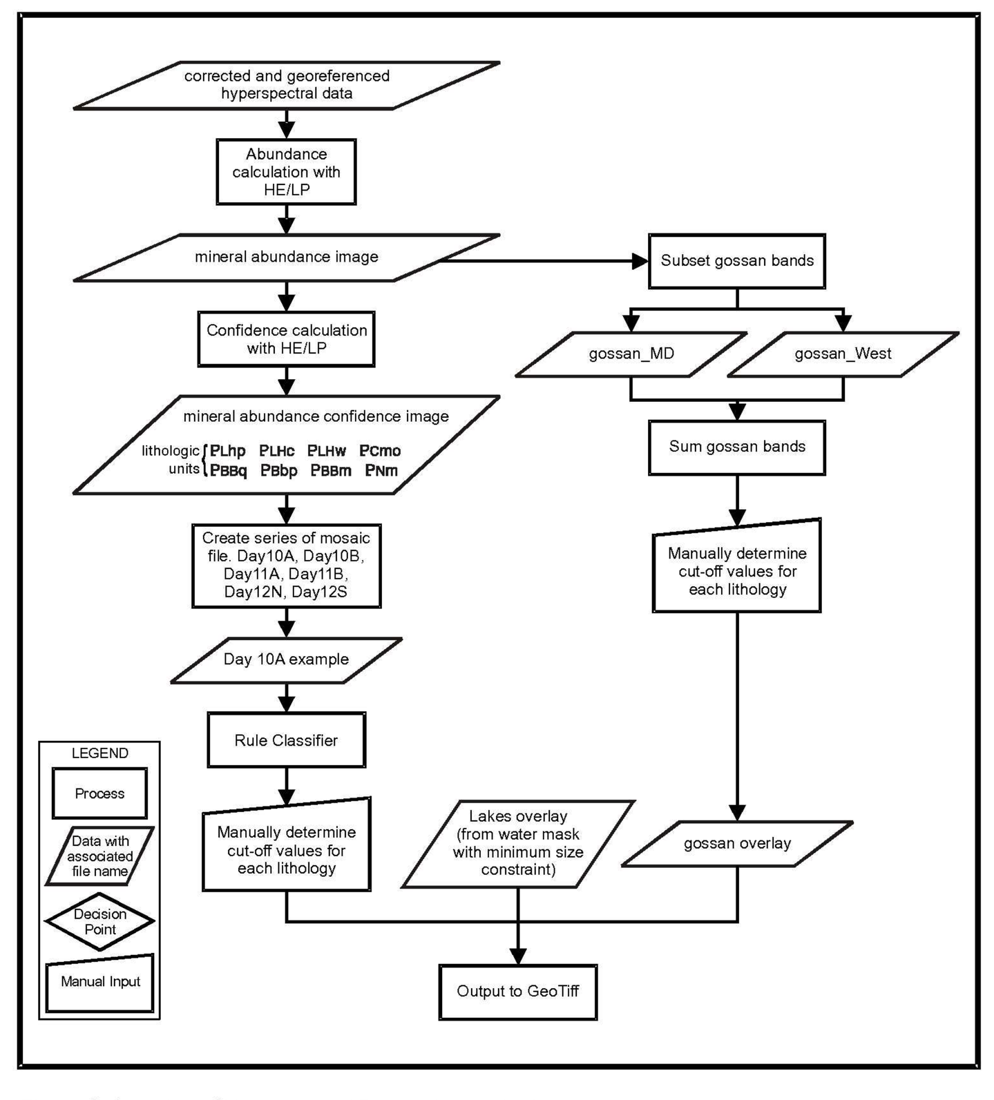

Figure 9. Overview of Hyperspectral Processing method.

Hyperspectral Maps

Figure 10 is an index map for the location of the hyperspectral data that comprise this series of 1:100,000 scale Open File maps. As can be seen, hyperspectral flight line coverage in each of the five map areas is incomplete. On each Open File map, the actual ground covered by the accepted flight lines is given. Within these areas, only the corresponding pixel locations that showed the best match to each end-member spectra are coloured according to legend (Fig. 8). The areas within the flight line coverage which remain unclassified to a lithological hyperspectral unit usually correlate to extensive till or vegetation cover.

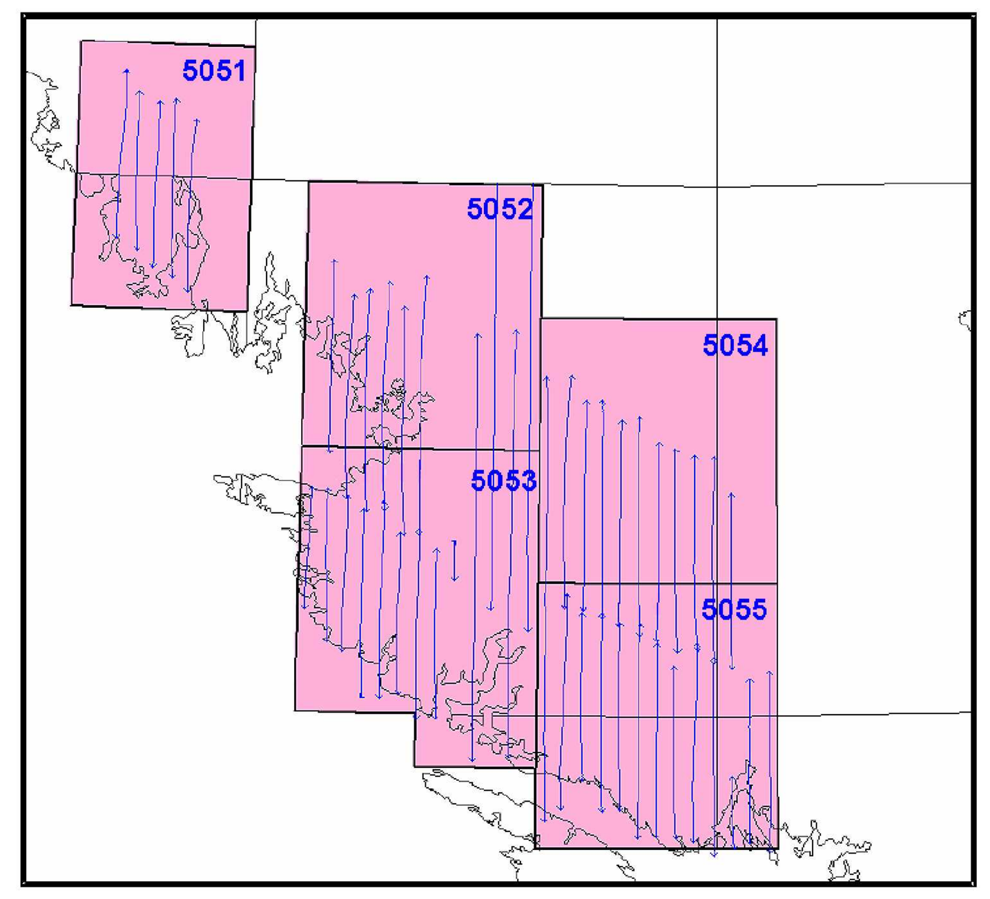

Figure 10. Location of each spectral map produced in this series of Open File maps.

REFERENCES - HYPERSPECTRAL

A.U.G. Signals Ltd.
2003: Report No: AUG-R&D-0104/03/FR/C, *New hyperspectral image processing tools for automatic discrimination of minerals*, CSA contract: 9F028-1-4900/08, October 2003.

Bowers,T.L. and Rowan, L.C.
1996: Remote mineralogic mapping of the Ice River complex, British Columbia, Canada, using AVRIS data, Photogrammetric Engineering and Remote Sensing, 62: pp. 1379–1385.

Budkewitsch, P., Staenz, K., Neville, R.A., Rencz, A. N., and Sangster, D.
2000: Spectral signatures of carbonate rocks surrounding the Nanisivik MVT Zn-Pb mine and implications of hyperspectral imaging for exploration in Arctic environments. Ore Deposit Workshop: New Ideas for a New Millenium, Technical Volume, East Kootenay Chamber of Mines, Cranbrook, BC, May 5-6, pp. 1–11.

Clarke, R.N., Gallagher, A., and Swayze, G.A.
1990: Material absorption and band depth mapping of imaging spectrometer data using a complete band shape least-squares fit with library spectra. *In* Proceedings of the second airborne visible/infrared imaging spectrometer (AVRIS) workshop. Edited by R.O. Green. NASA-JPL Publication 90-54, pp. 176–186.

Cloutis, E.A.
1992: Weathered and unweathered surface spectra of rocks from cold deserts: identification of weathering processes and remote sensing applications, Geologiska Föreningens i Stockholm Förhandlingar, 114: pp. 181–191.

Dempster, A.P.
1968: A generalization of Bayesian inference, Journal of the Royal Statistical Society, Series B, 30: pp. 205–247.

Duda, R., Hart, P., and Stork, P.
2001: Pattern Classification, John Wiley & Sons, Inc., New York, New York, 2nd edition.

Goetz, A.F.H., Rowan, L.C., and Kingston, M.J.
1982: Mineral identification from orbit: initial results from the shuttle multispectral infrared radiometer. Science, 218: pp. 1020–1031.

Harris, J.R., Eddy, B., Rencz, A.N., de Kemp, E., Budkewitsch, P., and Peshko, M.
2001: Remote sensing as a geological mapping tool in the Arctic: preliminary results from Baffin Island, Nunavut, Geological Survey of Canada, Current Research, 2001-E12: 1–9.

Harris, J.R., Rogge, D., Hitchcock, R., Ijewliw, O.E., and Wright D.
2005: Mapping lithology in Canada's Arctic: application of hyperspectral data using the minimum noise fraction transformation and matched filtering, Canadian Journal of Earth Science, 42: pp. 2173–2193.

Harsanyi, J.C. and Chang, C. I.
1994: Detection of low probability subpixel targets in hyperspectral image sequences with unknown backgrounds, IEEE Trans. Geoscience and Remote Sensing, 32: pp. 779–785.

Hunt, G.R.
1977: Spectral signatures of particulate minerals in the visible and near-infrared. Geophysics, 2: pp.501–513.

Hunt, G.R. and Salisbury, J.W.
1970: Visible and near-infrared spectra of mineral and rocks, I. Silicate minerals. Modern Geology, 1: pp. 283–300.
1971: Visible and near-infrared spectra of minerals and rocks, II. Carbonates. Modern Geology, 2: pp. 22–30.

Hunt, G.R., Salisbury, J.W., and Lenhoff, C.J.
1973a: Visible and near-infrared spectra of minerals and rocks, VI. Additional silicates. Modern Geology, 4: pp. 85–106.
1973b: Visible and near-infrared spectra of minerals and rocks, VI. Acid igneous rocks. Modern Geology, 4: pp. 217–224.
1974: Visible and near-infrared spectra of minerals and rocks, IX. Basic and ultra-basic igneous rocks. Modern Geology, 4: pp. 15–22.

Kelly, E.J.
1998: Fundamentals of Statistical Signal Processing, Volume 2: Detection theory, Prentice Hall, Upper Saddle River, New Jersey.

Lein, J.K.
2003: Applying evidential reasoning methods to agricultural land cover classification, International Journal of Remote Sensing, 24: pp. 4161–4180.

Rubicon Resources
1996: Geochemical and Geophysical Report on the Incognita JV Project 1996 Exploration Program, Meta Incognita Peninsula Baffin Island, NWT, Canada.

Shafer, G.
1976: A Mathematical Theory of Evidence, Princeton University Press, Princeton, New Jersey.

St-Onge, M.R., Scott, D.J., and Wodicka, N.
2001: Geology, Meta Incognita Peninsula, Baffin Island, Nunavut; Geological Survey of Canada, Map 2009A.

van der Meer, F. and de Jong, S.M. (Eds.)
2002: Imaging Spectrometry: Basic principles and prospective applications, Kluwer Academic Publishers, New York, New York.

DESCRIPTIVE NOTES - GEOLOGY

BEDROCK GEOLOGY: INTRODUCTION

The bedrock geology of southern Baffin Island between 68°W and 72°W is documented on a set of seven bedrock geological maps which present the results of 1:100 000 scale mapping by the Geological Survey of Canada (GSC) in the Frobisher Bay (Map 1979A), Hidden Bay (Map 1980A), McKellar Bay (Map 1981A), Wight Inlet (Map 1982A), Blandford Bay (Map 1983A), Crooks Inlet (Map 1984A), and White Strait (Map 1985A) map areas, Meta Incognita Peninsula, southern Baffin Island, Nunavut (St-Onge et al., 2001). To the west, the bedrock geology of the Mingo Lake–Macdonald Island area southern Baffin Island, Nunavut, is presented on GSC Map 1185A (Blackadar, 1967). An overview of the crustal architecture and tectonic evolution of the Meta Incognita Peninsula is presented in St-Onge et al. (2002, 2006). An outline of the deformation-metamorphism history for the Hudson Strait region is presented in St-Onge et al. (1999, 2000a, 2007). Scott (1997), Wodicka and Scott (1997), Scott and Wodicka (1998) and Scott et al. (2002) present U-Pb geochronological results for southern Baffin Island and highlight the distinct and/or common tectonic histories of different tectonostratigraphic assemblages. Examination of the surficial deposits at 1:100 000 scale and the identification of ice flow domains from the last (late Foxe) glaciation are outlined in Hodgson (1997) with surficial map units and structures documented on GSC maps 2042A–2048A (Hodgson, 2003). Geological work on southern Baffin Island prior to 1965 is summarized in Blackadar (1967).

NORTHEASTERN TRANS-HUDSON OROGEN

The metasedimentary rocks and orthogneisses of southern Baffin Island are part of the northeastern (Quebec-Baffin Island) segment of the Paleoproterozoic Trans-Hudson Orogen (Fig. 11; St-Onge et al., 2006), which comprises tectonostratigraphic assemblages accumulated on, or accreted to, the northern margin of the Archean Superior craton during more than 200 Ma of tectonic activity. Preserved within the northeastern segment of the orogen, from the external zone peripheral to the Superior craton in northern Quebec to the internal zone exposed on southern Baffin Island (Fig. 12) are the following tectonostratigraphic assemblages (St-Onge et al., 2002, 2006, and references therein): 1) lower plate parautochthonous plutonic and supracrustal rocks of the Archean Superior craton; 2) lower plate parautochthonous sedimentary and volcanic units (Povungnituk and Chukotat groups) associated with multiple Paleoproterozoic rifting events along the northern margin the Superior craton (St-Onge et al., 2000b and references therein); and 3) upper plate (i.e. allochthonous) Paleoproterozoic crustal elements interpreted as i) an ophiolite (Watts Group), ii) a fore-arc clastic apron (Spartan Group), iii) a magmatic arc terrane (Narsajuaq arc, Parent and Sugluk groups), iv) a clastic-carbonate platformal sequence and foreland basin sequence (Lake Harbour Group) and its potential crystalline basement (Ramsay River orthogneiss), and v) an extensive suite of monzogranitic plutons (Cumberland batholith), which intrude the platformal, basement and foreland basin rocks. A southern crustal suture (Bergeron suture; Fig. 12) separates the parautochthonous rocks of the Povungnituk and Chukotat groups from the allochthonous units of the Watts Group ophiolite, whereas a medial crustal suture (Soper River suture; Fig, 12) juxtaposes the allochthonous units of the Narsajuaq arc terrane against the platformal and foreland basin sequences of the Lake Harbour Group (St-Onge et al., 2006).

Uranium-lead (zircon) age determinations for plutonic units within the Superior craton basement of northern Quebec range between ca. 3.22–2.74 Ga (Parrish, 1989, R.R. Parrish, pers. comm., 1991; St-Onge et al., 1992; Scott and St-Onge, 1995; Wodicka and Scott, 1997). Rhyolite flows and gabbro sills from the Povungnituk and Chukotat groups (rift sequences) yield zircon and baddeleyite ages between ca. 2.04–1.96 Ga and 1.92–1.87 Ga, respectively (Parrish, 1989; St-Onge et al., 1992; Machado et al., 1993). Zircons from a gabbroic layer in the Watts Group (ophiolite) yield an age of ca. 2.00 Ga (Parrish, 1989). Plutons and felsic volcanic rocks of the Narsajuaq arc-Parent Group (magmatic arc terrane) in northern Quebec range in age between ca. 1.86–1.82 Ga (Parrish, 1989, R.R. Parrish, pers. comm., 1992; St-Onge et al., 1992; Machado et al., 1993; Scott, 1997; Wodicka and Scott, 1997; Scott and Wodicka, 1998), whereas monzogranite samples of the Cumberland batholith on Baffin Island yield ages between ca. 1.86–1.85 Ga (Jackson et al., 1990; Wodicka and Scott, 1997; Scott, 1999). Uranium-lead zircon geochronological constraints indicate that the Lake Harbour Group (platform and foreland basin sequences) were deposited between ca. 1.93 and 1.86 Ga (Scott and Gauthier, 1996; Scott, 1997; Scott et al., 1997, 2002). The potential depositional basement to the Lake Harbour Group (Ramsay River orthogneiss) has yielded a U-Pb age of ca. 1.95 Ga (Scott and Wodicka, 1998). Finally, metamorphism of the Lake Harbour Group is constrained between 1.85–1.83 Ga (M_1) and 1.82–1.81 Ga (M_2) (St-Onge et al., 2007).

META INCOGNITA PENINSULA

Meta Incognita Peninsula is characterized by three orogen-scale, stacked tectonic elements or levels (Fig. 13; Wodicka and Scott, 1997; St-Onge et al., 1999, 2002). From lowest to highest structural level, these include the following map units: level 1 - Superior craton basement and Povungnituk Group cover; level 2 - Narsajuaq arc terrane; level 3 - Ramsay River orthogneiss, Lake Harbour Group, and Cumberland batholith. The geological map pattern of Meta Incognita Peninsula (Fig. 13) is largely controlled by the interference between late orogenic, orogen-parallel folds (north- to northwest-trending) and cross folds (northeast-trending). On Big Island (north shore of Hudson Strait; Fig. 13), at the lowest structural levels exposed along the northeastern flank of a northwest-plunging, orogen-parallel anticlinorium underlying Hudson Strait, level 1 comprises Archean tonalite-granodiorite-monzogranite orthogneiss units and associated Paleoproterozoic clastic, mafic and ultramafic supracrustal rocks. The orthogneiss has been dated between 2.88–2.86 Ga (Wodicka and Scott, 1997) and is interpreted as correlative (and continuous) with metaplutonic units which belong to the Archean Superior craton of northern Quebec (Fig. 12; St-Onge et al., 1999, 2002). Based on lithological association, field characteristics, and mineral assemblages (St-Onge et al., 1996), as well as detrital zircon U-Pb age determinations (Scott et al., 2002), the Paleoproteorozoic cover units of level 1 are correlated with the Povungnituk Group rift margin units exposed south of Hudson Strait (Fig. 12; St-Onge et al., 1996, 1999). Between Hudson Strait and Frobisher Bay, at intermediate structural levels exposed along the antiformal hinge zone of a northeast-trending cross fold east of Kimmirut (Fig. 13), level 2 comprises layered monzogranite-granodiorite-tonalite gneiss with quartz diorite and rare anorthosite sheets. These units, which are dated between 1.84–1.82 Ga (Scott, 1997; Wodicka and Scott, 1997; Scott and Wodicka, 1998), have been correlated with the Narsajuaq arc in northern Quebec (Fig. 12; Scott, 1997). At the highest structural levels (level 3, Fig. 13), the Lake Harbour Group includes marble, psammite, quartzite, and semipelite that are intruded by mafic and locally layered mafic-ultramafic sills (Scott et al.,1997). Along the antiformal cross-fold hinge zone east of Kimmirut (Fig. 13), Lake Harbour Group supracrustal units are preserved within structural basins or klippen that result from the interference of the two regional fold sets. Within level 3, kilometre-scale panels of Lake Harbour Group rocks are imbricated with panels of Ramsay River orthogneiss (St-Onge et al., 2001). In a number of localities these imbricates are intruded by the monzogranite plutons of the Cumberland batholith.

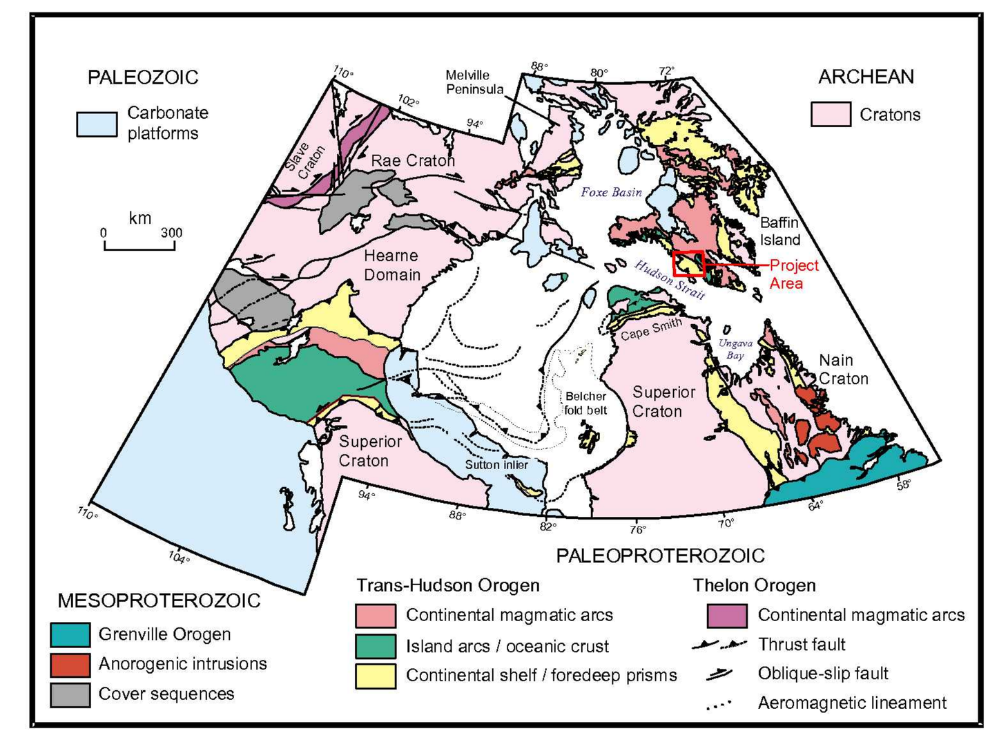

Figure 11. Geological map of northeastern Canada (modified from Wheeler et al., 1996) outlining the surface extent of the Trans-Hudson Orogen.

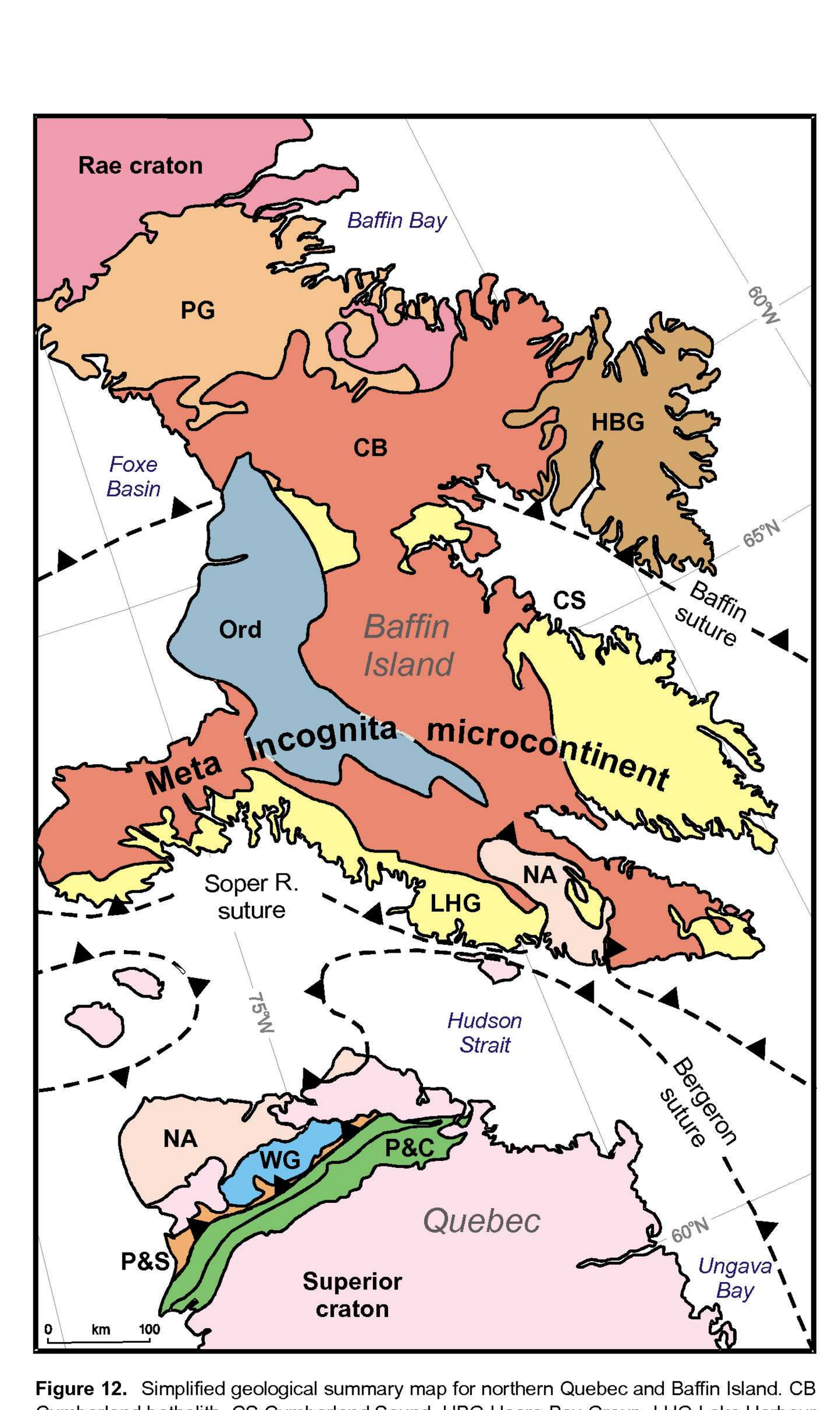

Figure 12. Simplified geological summary map for northern Quebec and Baffin Island. CB Cumberland batholith, CS Cumberland Sound, HBG Hoare Bay Group, LHG Lake Harbour Group and crystalline basement, NA Narsajuaq arc, Ord Ordovician cover, P&S Parent and Spartan groups, P&C Povungnituk and Chukotat groups, PG Piling Group, WG Watts Group.

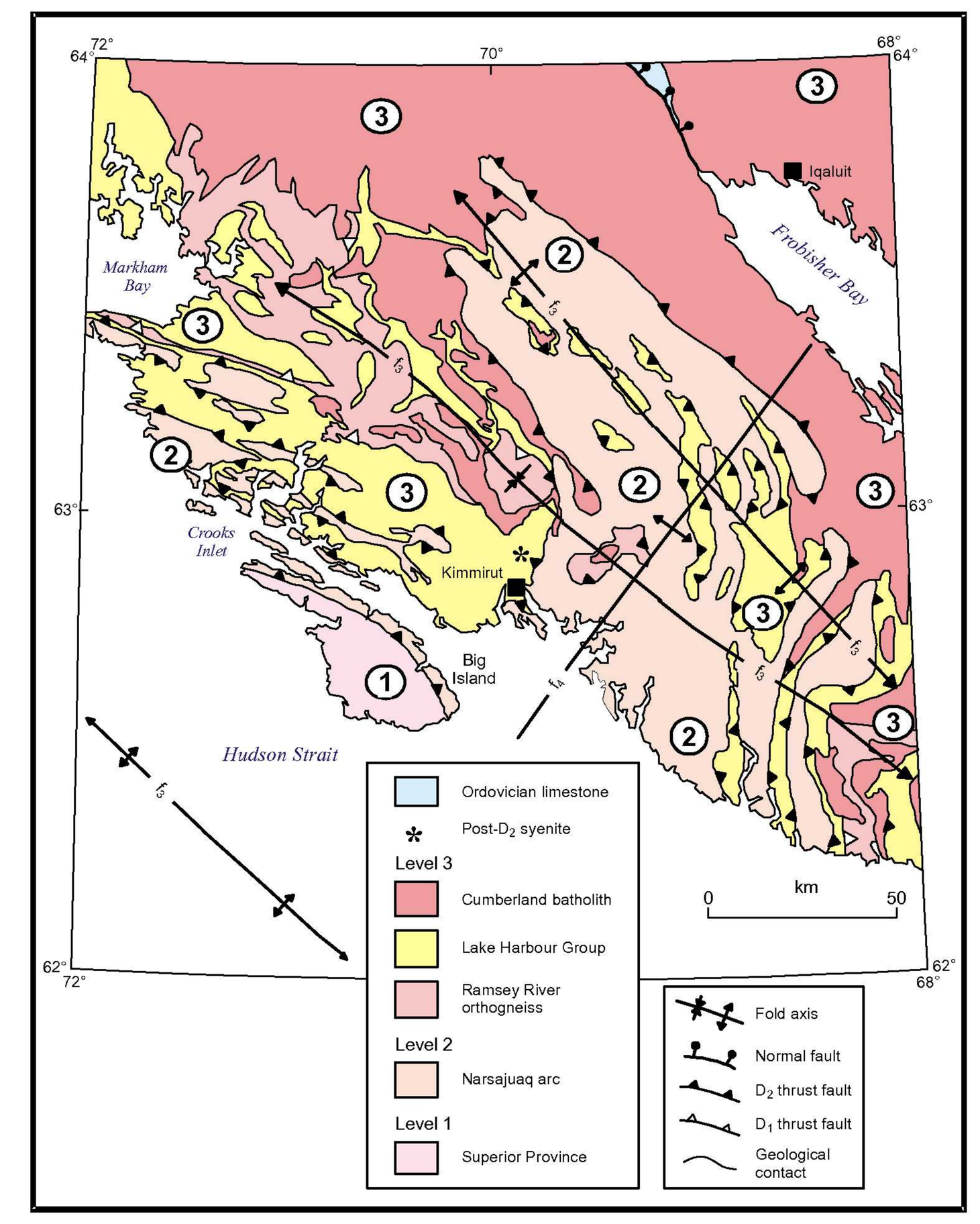

Figure 13. Generalized geology of southern Baffin Island between 68°W and 72°W, Meta Incognita Peninsula, Nunavut (after St-Onge et al., 2001), and identification of the principal structural levels (1–3) and crustal scale folds (f_3–f_4) described in the text.

REFERENCES - GEOLOGY

Blackadar, R.G.
1967: Geological reconnaissance, southern Baffin Island, District of Franklin; Geological Survey of Canada, Paper 66-47, 32 p.

Hodgson, D.A.
1997: Last glacial ice flows over western Meta Incognita Peninsula, southern Baffin Island, Northwest Territories; *in* Current Research 1997-C; Geological Survey of Canada, p. 179–184.
2003: Surficial geology, Meta Incognita Peninsula, Baffin Island, Nunavut; Geological Survey of Canada, Maps 2042A–2048A, 1:100 000 scale.

Jackson, G.D., Hunt, P.A., Loveridge, W.D., and Parrish, R.R.
1990: Reconnaissance geochronology of Baffin Island, N.W.T.; *in* Radiogenic Age and Isotopic Studies: Report 3; Geological Survey of Canada, Paper 89-2, p. 123–148.

Machado, N., David, J., Scott, D.J., Lamothe, D., Philippe, S., and Gariépy, C.
1993: U-Pb geochronology of the western Cape Smith Belt, Canada: new insights on the age of initial rifting and arc magmatism; Precambrian Research, v. 63, p. 211–224.

Parrish, R.R.
1989: U-Pb geochronology of the Cape Smith Belt and Sugluk block; Geoscience Canada, v. 16, p. 126–130.

Scott, D.J.
1997: Geology, U-Pb & Pb-Pb geochronology of the Lake Harbour area, southern Baffin Island: implications for the Paleoproterozoic tectonic evolution of NE Laurentia; Canadian Journal of Earth Sciences, v. 34, p. 140–155.
1999: U-Pb geochronology of the eastern Hall Peninsula, southern Baffin Island, Canada: a northern link between the Archean of West Greenland and the Paleoproterozoic Torngat Orogen of northern Labrador; Precambrian Research, v. 93, p. 5–26.

Scott, D.J. and Gauthier, G.
1996: Comparison of TIMS (U-Pb) and laser ablation microprobe ICP-MS (Pb) techniques for age determination of detrital zircons from Paleoproterozoic metasedimentary rocks from northeastern Laurentia, Canada, with tectonic implications; Chemical Geology, v. 131, p. 127–142.

Scott, D.J. and St-Onge, M.R.
1995: Constraints on Pb closure temperature in titanite based on rocks from the Ungava orogen, Canada: implications for U-Pb geochronology and P-T-t path determinations; Geology, v. 23, p. 1123–1126.

Scott, D.J. and Wodicka, N.
1998: A second report on the U-Pb geochronology of the Meta Incognita Peninsula, southern Baffin Island, Northwest Territories; *in* Radiogenic Age and Isotopic Studies, Report 11; Geological Survey of Canada, Current Research 1998-F, p. 47–57.

Scott, D.J., St-Onge, M.R., Wodicka, N., and Hanmer, S.
1997: Geology of the Markham Bay-Crooks Inlet area, southern Baffin Island, Northwest Territories; *in* Current Research 1997-C; Geological Survey of Canada, p. 157–166.

Scott, D.J., Stern, R.A., St-Onge, M.R., and McMullen, S.M.
2002: U-Pb geochronology of detrital zircons in metasedimentary rocks from southern Baffin Island: implications for the Paleoproterozoic tectonic evolution of Northeastern Laurentia; Canadian Journal of Earth Sciences, v. 39, p. 611–623.

St-Onge, M.R., Hanmer, S., and Scott, D.J.
1996: Geology of the Meta Incognita Peninsula, south Baffin Island: tectonostratigraphic units and regional correlations; *in* Current Research 1996-C; Geological Survey of Canada, p. 63–72.

St-Onge, M.R., Lucas, S.B., and Parrish, R.R.
1992: Terrane accretion in the internal zone of the Ungava orogen, northern Quebec. Part 1: tectonostratigraphic assemblages and their tectonic implications; Canadian Journal of Earth Sciences, v. 29, p. 746–764.

St-Onge, M.R., Scott, D.J., and Lucas, S.B.
2000b: Early partitioning of Quebec: Microcontinent formation in the Paleoproterozoic; Geology, v. 28, p. 323–326.

St-Onge, M.R., Scott, D.J., and Wodicka, N.
2001: Geology, Meta Incognita Peninsula, Baffin Island, Nunavut; Geological Survey of Canada, Map 2009A (containing Maps 1979A–1985A), 1:100 000 scale.
2002: Review of crustal architecture and evolution in the Ungava Peninsula–Baffin Island area: connection to the Lithoprobe ECSOOT transect; Canadian Journal of Earth Sciences, v. 39, p. 589–610.

St-Onge, M.R., Searle, M.P., and Wodicka, N.
2006: Trans-Hudson Orogen of North America and the Himalaya-Karakoram-Tibetan Orogen of Asia: Structural and thermal characteristics of the lower and upper plates; *Tectonics*, 25, doi:10.1029/2005TC001907, 22p.

St-Onge, M.R., Wodicka, N., and Ijewliw, O.
2007: Polymetamorphic evolution of Trans-Hudson Orogen on Baffin Island, Canada: constraints from petrology, structure, and geochronology. *Journal of Petrology*, 48, doi:1093/petrology/eg1060, 32p.

St-Onge, M.R., Wodicka, N., and Lucas, S.B.
2000a: Granulite- and amphibolite-facies metamorphism in a convergent-plate-margin setting: synthesis of the Quebec-Baffin segment of the Trans-Hudson Orogen; Canadian Mineralogist, v. 38, p. 379–398.

St-Onge, M.R., Lucas, S.B., Scott, D.J., and Wodicka, N.
1999: Upper and lower plate juxtaposition, deformation and metamorphism during crustal convergence, Trans-Hudson Orogen (Quebec-Baffin segment), Canada; Precambrian Research, v. 93, p. 27–49.

Wheeler, J.O., Hoffman, P.F., Card, K.D., Davidson, A., Sanford, B.V., Okulitch, A.V., and Roest, W.R.
1996: Geological Map of Canada; Geological Survey of Canada, Map 1860A, scale 1:5 000 000.

Wodicka, N. and Scott, D.J.
1997: A preliminary report on the U-Pb geochronology of the Meta Incognita Peninsula, southern Baffin Island, Northwest Territories; *in* Current Research 1997-C; Geological Survey of Canada, p. 167–178.

OPEN FILE
DOSSIER PUBLIC
5055
GEOLOGICAL SURVEY OF CANADA
COMMISSION GÉOLOGIQUE DU CANADA
2008
SHEET 2 OF 2
FEUILLET 2 DE 2

Open files are products that have not gone through the GSC formal publication process

Les dossiers publics sont des produits qui n'ont pas été soumis au processus officiel de publication de la CGC.

Sheet 2 of 2, Hyperspectral and Descriptive notes

Recommended Citation:
Peshko, M., Harris, J., Budkewitsch, P., St-Onge, M.R., McGregor, R., Hitchcock, R., and Desnoyers, D.
2008: Hyperspectral units, Soper Lake, Baffin Island, Nunavut; Geological Survey of Canada, Open File 5055, scale 1:100 000.